Computer Methods in Biomechanics and Biomedical Engineering

Virtualisation of stress distribution in heart valve tissue

Siyao Huang[a] & Hsiao-Ying Shadow Huang[a]

[a] Mechanical and Aerospace Engineering Department, North Carolina State University, 3002 EBIII, Campus Box 7910, 911 Oval Drive, Raleigh, NC 27695-7910, USA
Published online: 12 Mar 2013.

PLEASE SCROLL DOWN FOR ARTICLE

Taylor & Francis
Taylor & Francis Group

Virtualisation of stress distribution in heart valve tissue

Siyao Huang and Hsiao-Ying Shadow Huang*

Mechanical and Aerospace Engineering Department, North Carolina State University, 3002 EBIII, Campus Box 7910, 911 Oval Drive, Raleigh, NC 27695-7910, USA

This study presents an image-based finite element analysis incorporating histological photomicrographs of heart valve tissues. We report stress fields inside heart valve tissues, where heterogeneously distributed collagen fibres are responsible for transmitting forces into cells. Linear isotropic and anisotropic tissue material property models are incorporated to quantify the overall stress distributions in heart valve tissues. By establishing an effective predictive method with new computational tools and by performing virtual experiments on the heart valve tissue photomicrographs, we clarify how stresses are transferred from matrix to cell. The results clearly reveal the roles of heterogeneously distributed collagen fibres in mitigating stress developments inside heart valve tissues. Moreover, most local peak stresses occur around cell nuclei, suggesting that higher stress may be mediated by cells for biomechanical regulations.

Keywords: heart valve tissue; finite element method; collagen fibre architecture; stress analysis

1. Introduction

It is estimated that 250,000 Americans currently suffer from heart valve diseases (NIH 2010; Roger et al. 2012). Therefore, the need to understand the homeostasis of healthy valvular tissue, its dependence on cellular mechanotransduction and mechanisms of pathogenesis is vital. Studies have shown that heart valve diseases are caused by disrupted tissue homeostasis in the valvular extracellular matrix (ECM) under a variety of pathological conditions, resulting in alterations in heart valve microstructures, mechanical properties and other biomechanical regulations (Mays et al. 1988; Fung 1993; Durbin and Gotlieb 2002; Durbin et al. 2005; Fayet et al. 2007; Porter and Turner 2009). This is the key obstacle faced for healthy cardiovascular function, hindering the survival and quality of life of many patients. It has been suggested that valvular ECM and cell functions are modulated by mechanical forces and stretches (Carver et al. 1991; Choquet et al. 1997; Sheetz et al. 1998; Atance et al. 2004; Huang et al. 2007; Puklin-Faucher and Sheetz 2009; Lewinsohn et al. 2011), where tissues respond to the mechanical environment by growth and remodelling, repair and degradation, and cells provide adaptive responses, such as the synthesis and secretion of cytokines, growth factors, and differentiation to other phenotypes (Nakagawa et al. 1989; Mulholland and Gotlieb 1996, 1997; Taylor et al. 2000, 2003; Porter and Turner 2009). It has been demonstrated that valve interstitial cells (VICs) play a significant role in the maintenance and regeneration of heart valves (Mulholland and Gotlieb 1996, 1997;

Taylor et al. 2000, 2003; Latif et al. 2006). Thus, there is a critical need to understand matrix–cell interactions.

Recently, tissue engineering has been considered as a potential treatment for heart valve replacements. Derived from autologous cells seeded and grown on a polymer scaffold, the engineered tissue has the features of self-acting tissue repair and remodelling, which are different from conventional replacements (El Khoury et al. 2006; Mendelson and Schoen 2006; El Oakley et al. 2008), and the impact from rejections of blood and tissue type no longer takes place. However, even if tissue-engineered heart valves have been achieved *in vitro* (Engelmayr et al. 2003, 2005, 2006), the difficulties for tissue-engineered heart valve development still exist in growing a native-like heart valve, which is able to function compatibly with native ones.

The microstructure and mechanical properties of native heart valves are physically critical factors in modelling valve tissue equivalents. The specific collagen network and numerous cells distributed over the heart valve tissue result in an inhomogeneous heart valve microstructure and a non-linear anisotropic material property for the heart valve (Sacks et al. 1998; Billiar and Sacks 2000a; Doehring et al. 2005; Joyce et al. 2009). Collagen fibre orientation and impaction in the circumferential direction during heart valve functioning can resist more deformation in the circumferential direction (Sacks et al. 1998; Huang et al. 2007; Joyce et al. 2009; Cox et al. 2010); in contrast, heart valve tissue in the radial direction is more compliant. The response of the heart valve to external loading is anisotropic, and it is mainly due to

*Corresponding author. Email: hshuang@ncsu.edu

collagen fibre architecture (Sacks et al. 1998, 2009; Huang et al. 2007; Joyce et al. 2009; Cox et al. 2010).

To investigate such microstructural responses of the heart valve in a mechanical environment, computational simulations of heart valve tissues via finite element analysis (FEA) have been widely applied, given a simplified homogeneous finite element model to represent a highly heterogeneous collagen fibre network (Li et al. 2001; Luo et al. 2003; Mohammadi et al. 2009; Koch et al. 2010). In simplified homogeneous elastic finite element models, the stress distribution on the valve leaflet via FEA has illustrated the relationship between the collagen fibre orientations, fibre bundle locations and local stresses, suggesting that the stress distribution is highly dependent on the collagen fibre distribution (Li et al. 2001; Luo et al. 2003; Mohammadi et al. 2009; Koch et al. 2010). Some geometric parameters are also regarded as important factors for the mechanical behaviour of heart valve tissues, such as leaflet diameters and thickness (Li et al. 2001; Carew et al. 2003; Luo et al. 2003; Mohammadi et al. 2009; Koch et al. 2010).

Furthermore, isolated VICs are usually subjected to strain via a mechanical tension system or quantified indirectly via confocal microscopy with the linear elasticity approximation (Lewinsohn et al. 2011). VIC-mediated contraction is further observed to be responsive to various growth factors and is speculated to influence tissue mechanical properties. Moreover, it is observed that VICs express different phenotypes with distinct morphologies when seeded in matrices with different stiffnesses in calcifying media (Yip et al. 2009). Isolated VICs have been observed to be sensitive to their mechanical environment and responsible for cell–cell and cell–ECM communications, as well as ECM maintenance (Mulholland and Gotlieb 1996, 1997; Taylor et al. 2000, 2002, 2003; Latif et al. 2005, 2006; Chester and Taylor 2007; Liu et al. 2007). While these experimental approaches have successfully demonstrated that ECM–VIC mechanical interactions play significant roles in tissue homeostasis, it is clear that enabling the visualisation of stress distributions inside biological systems under physiological mechanical stimuli will yield a greater level of understanding of biomechanical regulation in biological systems. Previous studies are valuable for understanding mechanical behaviours in the heart valve tissues (Billiar and Sacks 2000b; Sun et al. 2005; Stella and Sacks 2007; Koch et al. 2010). However, complete descriptions of heart valves cannot be delineated in a good manner by simplified homogeneous finite element models or a mechanism from isolated VICs. Therefore, this study demonstrates that an image-based finite element method with customised functionalities simulates heterogeneous collagen fibre microstructures and VIC populations, and further matrix-to-cell stress transfer is virtualised and visualised in heart valve tissues.

2. Materials and methods

2.1 Photomicrograph preparation

In this study, we chose to use standard histological photomicrographs in our image-based biomechanics study because microstructures of ECM and cells could be preserved for microscopic investigation. In brief, porcine pulmonary valve leaflet samples were fixed in 10% (v/v) buffered formalin, paraffin embedded, sectioned and stained with haematoxylin and eosin (H&E), and the histological slides were digitised as photomicrographs via an optical microscope (Huang et al. 2007, 2012). Because the field of view of the microscope at the required magnification for high-resolution imaging was limited, panoramic images based on the said high-resolution photomicrographs were generated by digital concatenation to span the entire tissue sample area of interest. Panoramic images were constructed from four to five overlapped photomicrographs; to render a sufficiently high-quality panoramic image, a span of overlap of 50–70% was required. The panoramic photomicrograph images revealed the microstructures of the ECM and VICs. For details, please refer to Huang et al. (2007).

2.2 Image-based finite element analysis

Because of the difficulty in describing the microstructure in conventional FEA packages, simplified and homogenised models are built to investigate microstructural behaviour. Different from conventional FEA software, the Object-Oriented Finite Element (OOF) software developed by the National Institute of Standards and Technology (Gaithersburg, MD, USA) is applied to the analysis of the properties of generic microstructures (Langer et al. 2001; Reid et al. 2009). By capturing a digital microstructural photomicrograph where heterogeneous collagen fibre architecture and cell population are preserved and visualised, OOF can create an image-based FEA model with material properties specified in the selected pixel groups on the image.

OOF is written in a blend of C++ and Python: Python is used heavily for the user interface, whereas C++ is reserved for performance-critical code blocks, especially those that tend to be computationally intensive. To ensure that all pixels in the images are assigned to a pixel group, the study builds a pixel selection extension, whereas an extension is a group of discrete packets of code and the said extension can dynamically interact with a host program as it executes. The developed pixel selection extension integrates with the current OOF code to better facilitate FEA for heart valve tissues. When OOF solves a finite element problem, it is necessary to have all the pixels in an image assigned to a particular pixel group and thereby associated with particular material properties. Should any pixels be missed, the results of the analysis will
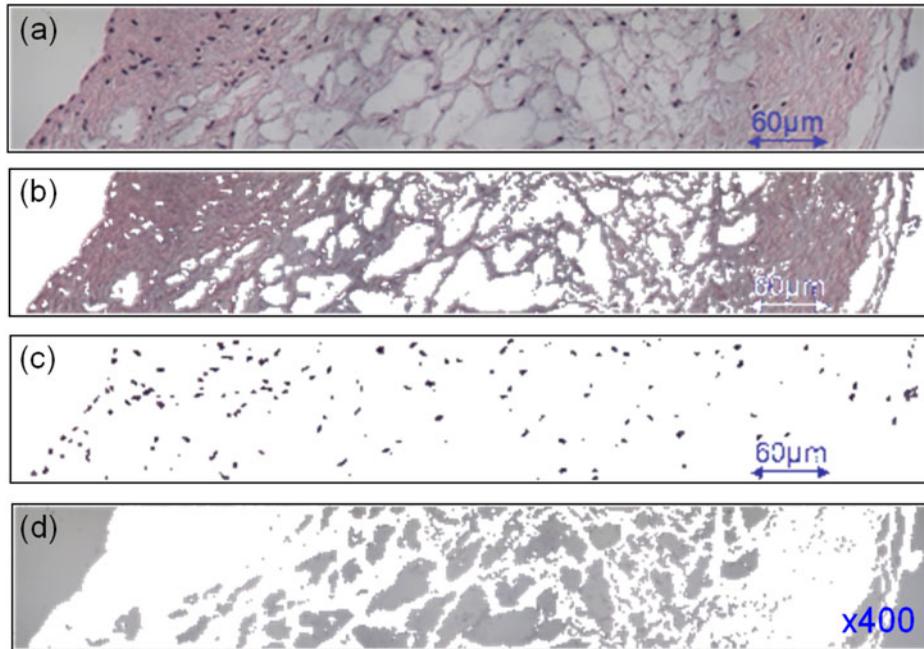
Figure 1. The developed pixel selection extension based on the HSI colour space. (a) Original histological photomicrograph of heart valve tissue. (b) Only stained collagen fibers are selected from the original image. (c) Only stained nuclei are selected from the original image. (d) Only empty space is selected from the original image. The extension ensures that all pixels in the images are assigned to their appropriate pixel groups. The function of the pixel selection extension is to facilitate material property assignments in the FEA process. Scale bar = 60 μm, original magnification, 400 ×.

include 'holes', where no material properties have been defined. The extension uses the properties of the colours in the image to distinguish between various objects in the image. The hue–saturation–intensity (HSI) colour space represents colours as a combination of the following: (1) the shade of a colour (i.e. hue), such as blue, green, red, yellow. (2) The vibrancy of the colour (i.e. saturation); colours with a low saturation appear to be pale or 'washed out'. For example, a red hue with a reduced saturation is pink. (3) The intensity of the colour, which refers to the brightness of the colour, with zero intensity representing fully dark (i.e. black). In photomicrographs of H&E-stained porcine heart valve tissue, it has been readily observed that VIC nuclei (stained dark blue by haematoxylin) are associated with a low intensity (compared with voids appearing as transparent regions in the photomicrograph), whereas collagen fibres manifest a relatively high saturation (Figure 1). The extension is developed and implemented in two parts: (a) the courier (written in C++) iterates through the pixels of the entire image and uses the comparator to compare the value of the component with the threshold, whereas a comparator is one of function-object classes in the Standard C++ Library. Specifically, a comparator works as comparing two values or arguments, and it returns a Boolean value. The returned value should be true if the first argument must precede the second, and false otherwise. Once the comparison is true, then the pixel is added to the

selection. (b) The second part is written in Python and receives values from the user interface for use in constructing the courier. The extension helps ensure that all pixels in the images are assigned to their appropriate pixel groups and the developed pixel selection extension facilitates material property assignments in the later FEA process.

2.3 Virtual experiments on heart valve tissue histological photomicrographs

The virtual experiments employ finite element methods to simulate physiologically relevant biaxial stretching states on tissues and depict changes in collagen fibre orientations and the resultant cellular stress environment (Figure 2). Because two-dimensional histological photomicrographs are used in our study (Figure 2(a)), the plane stress condition is assumed in the finite element analyses. A 500 × 500-pixel image of an en-face pulmonary valve leaflet photomicrograph is used for simulations with 30% of strain stretching equibiaxially (Figure 2(b)). Quad-rilateral plane stress elements are used in our finite element models. The pixel is the unit used in our finite element models; therefore, a 500 × 500-pixel finite element model with 30% equibiaxial stretching is equivalent to a 150-pixel displacement stretching in all directions (Figure 2(c)). To illustrate the stress transfer because of heterogeneous collagen fibre architecture and the
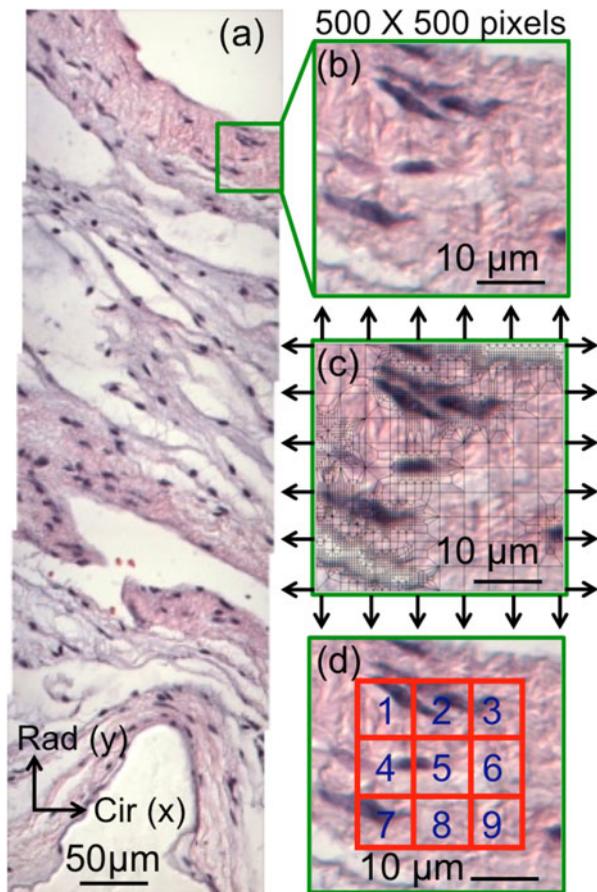
Figure 2. Virtual experiments on a pulmonary heart valve tissue histological photomicrograph. Circumferential (x) and radial (y) directions are denoted. (a) An en-face H&E-stained tissue leaflet photomicrograph. (b) A section of interest with 500×500 pixels. (c) Applying boundary conditions on the meshed image. (d) Obtaining calculated stress fields in nine regions in the selected image, $400 \times$.

anisotropic material property, this study conducts two sets of virtual experiments: (a) Linear isotropic material property is assumed and adopted in collagen fibres: $E = E_x = E_y = 408$ kPa, $\nu = 0.45$. The value is obtained from our experimental result around 30% biaxial stretching (Huang et al. 2012). It is aimed to delineate the effects of heterogeneous collagen fibre architecture. (b) Anisotropic material property for the collagen fibres is used, and the material property is obtained and derived from our previous experimental findings (Huang et al. 2012). It is well recognised that heart valve tissues experience large deformation during cardiac cycles. A piecewise linear elastic material properties during 28–35% of equibiaxial stretching ($E_x = 1457.19$ kPa, $E_y = 172.44$ kPa and $\nu_{12} = 0.45$) (Huang et al. 2012) are used to obtain the stiffness matrix (Nye 1957; Slaughter, 2001; Huang and Huang 2012). Therefore, $C_{11} = 1493$ kPa, $C_{12} = C_{21} = 79$ kPa, $C_{22} = 176$ kPa and $C_{66} = 217$ kPa

are adopted in the anisotropic finite element model. Cell nuclei are assumed to be isotropic materials, and $E = 0.9$ kPa and $\nu = 0.45$ are adopted (Huang et al. 2007). It is well recognised, however, that biological tissues or cardiac cells such as VICs are viscoelastic (Park et al. 2005; Lim et al. 2006; Janmey and McCulloch 2007). Considering that the time period of cardiac loading is ~ 400 ms, any viscoelasticity of tissues and cells is not expected to contribute significantly to simulation predictions. Voids are also assumed to be isotropic materials with $E = 0.01$ kPa and $\nu = 0.45$. Moreover, to better visualise and quantify the stress transfer between ECM and cell nuclei, nine regions are defined as shown in Figure 2(d). Stress fields at each integration point in the 500×500-pixel finite element models are calculated.

3. Results and discussion

The FEA results depict the effects of the inhomogeneous collagen fibre architectures while samples are under 30% strain due to equibiaxial stretching. The contours of displacements for isotropic and anisotropic models are shown in Figure 3. The displacement in the y-direction of the isotropic models reveals how collagen fibre distribution affects displacement contours, as shown in Figure 3(b). In general, a homogenised finite element model with isotropic material properties would provide displacement gradients parallel to the stretching/loading directions. Because our models incorporate heterogeneous microstructures, the results are distinct from other studies that do not consider collagen fibre architectures and cell distributions. From our selected sample (Figure 2(b)), voids are located in the upper right and lower left corners, and therefore, collagen fibres are shifted normal to these directions because of the low stiffness of voids: a displacement gradient in the y-direction then appears to be somewhat parallel to the x-direction. Moreover, less displacement is observed in the anisotropic models in the x-direction, which is because of the stiffness matrix: the components contributing to the x-direction are stiffer than those in the isotropic models. Although the components contributing to the y-direction are more pliable than those in the isotropic models, less displacement in the y-direction is also observed in the anisotropic models. It is concluded that circumferential collagen fibres have constrained the deformation in the radial direction, the y-direction. Therefore, complete descriptions of heart valves could be delineated by finite element models incorporating heterogeneous collagen fibres and cell distribution.

To better visualise how mechanical stresses are transferred from ECM to cell nuclei under 30% strain stretching equibiaxially, stress fields for both isotropic and anisotropic models are shown in Figure 4. Figure 4 (a)–(c) presents stress fields in the isotropic finite element models,
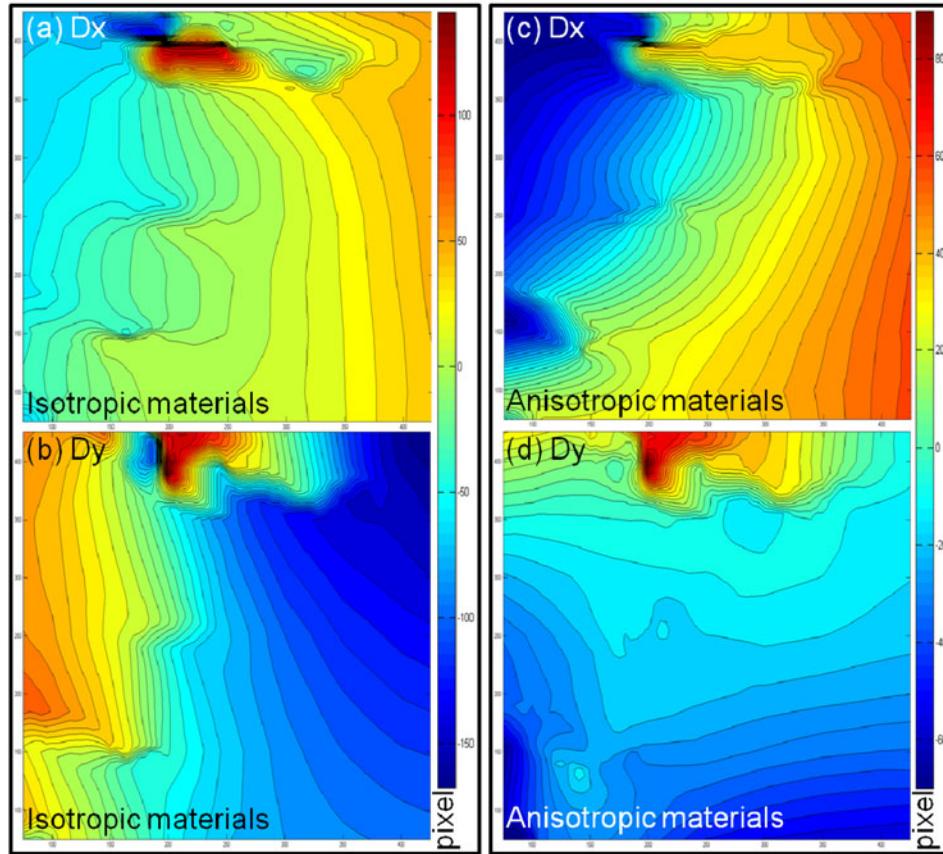
Figure 3. (a), (b) Contours of displacement in *x*- and *y*-directions for isotropic models. Colour key: blue $= -150$ (pixel) and red $= 150$ (pixel). (c), (d) Contours of displacement in *x*- and *y*-directions for anisotropic models. Colour key: blue $= -70$ (pixel) and red $= 90$ (pixel). Less displacement is observed in the anisotropic models in the *x*-direction because of the stiffness matrix: the components contributing to the *x*-direction are stiffer than those in the isotropic models. However, the components contributing to the *y*-direction are more pliable than those in the isotropic models; less displacement in the *y*-direction is also observed in the anisotropic models. It is concluded that circumferential collagen fibres have constrained the deformation in the radial direction, the *y*-direction.

and Figure 4 (d)–(f) presents stress fields of the anisotropic finite element models under 30% equibiaxial stretching. In addition, two locations are selected to represent the mechanical interaction between ECM and cells for both isotropic and anisotropic models. Stress values at selected locations are shown in Table 1 and Figure 4 to delineate the effects of collagen fibre architectures and material properties.

Stress concentrations of σ_{xx} are observed around the perimeters of cell nuclei in Figure 4(a). However, smaller stress concentrations for σ_{yy} are found in Figure 4(b). Because $E_x = E_y = 408$ kPa are used for the isotropic models, the different values and locations of stress concentrations are mainly attributed to the inhomogeneous collagen fibre and cell nuclei distributions. Shear stresses are shown in Figure 4(c), and different locations of peak

Table 1. A comparison of stress fields at two locations with two material properties inside heart valve tissue photomicrographs.

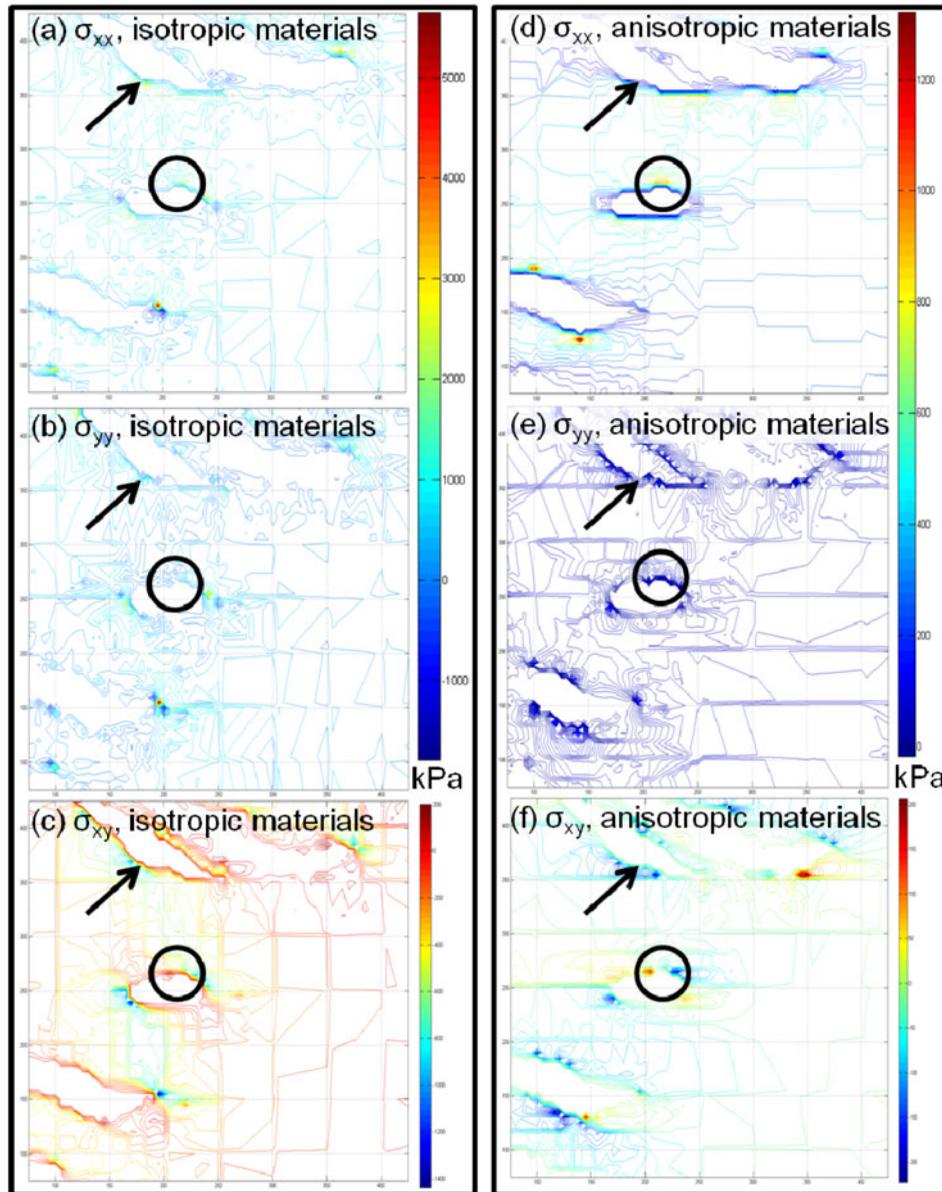| Stress fields	Location 1 (185, 360)		Location 2 (220, 270)	
	Isotropic materials (kPa)	Anisotropic materials (kPa)	Isotropic materials (kPa)	Anisotropic materials (kPa)
σ_{xx}	3361.82	753.03	2231.11	978.68
σ_{yy}	1635.81	86.93	967.82	84.06
σ_{xy}	−781.95	−192.21	−733.53	−96.69

Figure 4. Stress concentrations are observed around perimeters of cell nuclei, and the associated values are different at selected locations, where location 1 with coordinates (185, 360) is denoted by an arrow and location 2 with coordinates (220, 270) is denoted by a circle. (a), (b) Isotropic finite element models under 30% equibiaxial stretching. $\sigma_{xx} = 3361.82$ kPa and $\sigma_{yy} = 1635.81$ kPa at location 1. $\sigma_{xx} = 2231.11$ kPa and $\sigma_{yy} = 967.82$ kPa at location 2. Colour key: blue $= -1500$ kPa and red $= 5500$ kPa. (c) $\sigma_{xy} = -781.95$ kPa at location 1 and $\sigma_{xy} = -733.53$ kPa at location 2. Colour key: blue $= -1400$ kPa and red $= 200$ kPa. (d),(e) Anisotropic finite element models under 30% equibiaxial stretching. $\sigma_{xx} = 753.03$ kPa and $\sigma_{yy} = 86.93$ kPa at location 1. $\sigma_{xx} = 978.68$ kPa and $\sigma_{yy} = 84.06$ kPa at location 2. Colour key: blue $= 0$ kPa and red $= 1300$ kPa. (f) $\sigma_{xy} = -192.21$ kPa at location 1 and $\sigma_{xy} = -96.69$ kPa at location 2. Colour key: blue $= -200$ kPa and red $= 200$ kPa. Stress values are also listed in Table 1 to aid comparison.

shear stresses are observed, compared with the ones in Figure 4(a),(b). Based on the nature of isotropic materials, it is suggested that inhomogeneous collagen fibre architectures and cell nuclei distribution play a significant role in how stresses are transferred from ECM to cell nuclei.

From Figure 4(d),(e), smaller values in stresses are observed compared with those in the isotropic models.

Stress concentrations are observed around the perimeters of cell nuclei, and the locations are very different from ones from the isotropic models. σ_{yy} in Figure 4(e) has a smaller value than σ_{xx} in Figure 4(d), mainly because of the stiffness matrix: the components contributing to the *x*-direction are stiffer than those contributing to the *y*-direction in the anisotropic models. The distribution of the stress concentrations is also different from those

observed in Figure 4(d) of the anisotropic model and Figure 4(b) of the isotropic model. Shear stresses σ_{xy} in the anisotropic finite element model via 30% equibiaxial stretching are also reported (Figure 4(f)). Different locations for the stress concentration are observed, compared with the ones in the isotropic model in Figure 4(c). Smaller σ_{xy} values in the anisotropic models than ones in the isotropic model are also observed. It is further suggested that stress distribution in biological tissues and ECM–cell stress transfer could be greatly delineated via simulations incorporating anisotropy material property, inhomogeneous collagen fibre architectures and cell nuclei distribution.

Stress values at selected locations further revealed the effects of collagen fibre architectures and material properties (Table 1). A location indicated by an arrow with coordinates (185, 360) has stresses of $\sigma_{xx} = 3361.82$ kPa, $\sigma_{yy} = 1635.81$ kPa and $\sigma_{xy} = -781.95$ kPa for models using isotropic material properties (Table 1). Finite element models with anisotropic material properties at the same location has stresses of $\sigma_{xx} = 753.03$ kPa, $\sigma_{yy} = 86.93$ kPa and $\sigma_{xy} = -192.21$ kPa (Table 1). It is suggested that anisotropic material properties mitigate stress formation in heart valve tissues. Moreover, the circled location with coordinates (220, 270) has stresses of $\sigma_{xx} = 2231.11$ kPa, $\sigma_{yy} = 967.82$ kPa and $\sigma_{xy} = -733.53$ kPa for models using isotropic material properties (Table 1). The stress fields at this location for tissue with anisotropic material properties are $\sigma_{xx} = 978.68$ kPa, $\sigma_{yy} = 84.06$ kPa and $\sigma_{xy} = -96.69$ kPa (Table 1). Similar trends of stress relaxation are observed in models using anisotropic materials. Comparing two selected locations where location 2 is further away from the boundary, it is expected that lower stresses would be found in location 2 for isotropic models. However, a different result is found in anisotropic models, in which the σ_{xx} and σ_{yy} values for locations 1 and 2 are comparable (less location dependent). Interestingly, the ratio of stresses between the x- and y-directions are between 2 and 3 for isotropic materials ($\sigma_{xx}^{I} / \sigma_{yy}^{I} = \sim 2$) and are between 9 and 11 for anisotropic materials ($\sigma_{xx}^{A}/\sigma_{yy}^{A} = 9 - 11$), regardless of the selected locations.

4. Conclusions

To the authors' knowledge, this is the first study reporting stress fields inside porcine heart valve tissues. The FEAs incorporate collagen fibre and cell nuclei distributions, in addition to the measured anisotropic material properties (Huang et al. 2012). A number of FEA studies have utilised elastic isotropic or anisotropic materials, and their results suggest that the stress distribution is highly dependent on collagen fibre distribution (Li et al. 2001; Luo et al. 2003; Mohammadi et al. 2009; Koch et al. 2010). However, the homogeneous collagen fibre distri-

butions generally adopted in these studies exclude any cells in the models. Here, we demonstrate a different approach by incorporating both microstructure and anisotropic material properties, and the study discusses how the aforementioned properties affect the stress fields of cells inside ECM. This study provides stress distribution in biological tissues and ECM–cell stress transfer via simulations. The result shows that collagen fibre architectures, cell nuclei distribution and anisotropic material properties are key factors in the transfer of stresses from ECM to the cells inside heart valve tissues. A parametric study incorporating changes in the orthogonal stiffness matrices at different stages of strain stretching (0–18%, 18–28% and 28–35%) was conducted and published elsewhere (Huang and Huang 2013). The aim was to further understand the important effects of changing anisotropic material properties during cardiac cycles.

Moreover, several studies have used different imaging systems to delineate collagen fibre architectures in heart valve tissues: the small-angle light scattering method utilises a 4-mW HeNe ($\lambda = 632.8$ nm) continuous unpolarised wave laser to gain information about tissue structure (Sacks et al. 1998). Polarised light microscopy is used to visualise the heart valve tissue leaflets at the intermediate scale, and branching fibre bundles and membrane structure could be easily observed (Doehring et al. 2005). Furthermore, polarimetric fibre alignment imaging systems are used to bridge between *in vitro* collagen fibre distribution measurements and *in silico* multiscale modelling of heart valve tissues. Nevertheless, cell populations are excluded from these images. In contrast, we have incorporated randomly distributed cell nuclei from the histological photomicrographs and therefore better depict stress distributions inside heart valve tissues.

This study is able to reveal the roles of heterogeneously distributed collagen fibres and anisotropic materials in mitigating stress developments inside heart valve tissues (Figure 4). Different stress distributions in the circumferential and radial directions are clear from the isotropic models (Figure 4(a),(b)), whereas anisotropic models exhibit similar behaviours in the stress distribution in the circumferential and radial directions (Figure 4(d),(e)). Moreover, most local peak stresses observed in both directions occur around cell nuclei. Because cells are generally more pliable than ECM, such higher stress values may be mediated by cells for biomechanical regulations.

It is known that the internal inhomogeneous composition, such as cell distribution, has a great influence on the mechanics of the heart valve, such as the deformation of VICs (Huang et al. 2007; Langevin et al. 2010). VICs are regarded as regulators associated with synthesising and maintaining the valvular ECM to provide a structural

framework that is because of the unique profiles of molecular expression in cell–cell and cell–ECM adhesion, as well as the observation that age-related decreases in VIC numbers accompany collagen fibre degeneration (Latif et al. 2005, 2006). The abilities of VICs to communicate with each other and with the ECM and to respond to their environment basically support the mechanisms that allow heart valves to function in an optimal and efficient manner (Chester and Taylor 2007). Furthermore, structure–mechanics–property relations are tightly coupled in the biomechanical regulation of the tissue homeostasis induced by the alterations in cellular phenotype and morphology (Mays et al. 1988; Fung 1993; Durbin and Gotlieb 2002; Fayet et al. 2007). It has been observed that VICs are sensible to the mechanical environment, and the VICs' phenotypes and functions can be changed to mediate the tissue microstructure by mechanical stimuli (Choquet et al. 1997; Schwarzbauer 1997; Sheetz et al. 1998; Atance et al. 2004; Huang et al. 2007; Puklin-Faucher and Sheetz 2009). These facts suggest that ECM and cell functions are modulated by mechanical forces and stretches. Therefore, the result of this study helps provide insights into alterations in heart valve microstructure, mechanical properties and other potential biomechanical regulations resulting from heart valve diseases, which are caused by the disrupted tissue homeostasis under a variety of pathological conditions.

References

Atance J, Yost MJ, Carver W. 2004. Influence of the extracellular matrix on the regulation of cardiac fibroblast behavior by mechanical stretch. J Cell Physiol. 200:377–386.

Billiar KL, Sacks MS. 2000a. Biaxial mechanical properties of the natural and glutaraldehyde treated aortic valve cusp – part I: Experimental results. J Biomech Eng. 122:23–30.

Billiar KL, Sacks MS. 2000b. Biaxial mechanical properties of the native and glutaraldehyde-treated aortic valve cusp: part II – a structural constitutive model. J Biomech Eng. 122:327–335.

Carew EO, Patel J, Garg A, Houghtaling P, Blackstone E, Vesely I. 2003. Effect of specimen size and aspect ratio on the tensile properties of porcine aortic valve tissues. Ann Biomed Eng. 31:526–535.

Carver W, Nagpal ML, Nachtigal M, Borg TK, Terracio L. 1991. Collagen expression in mechanically stimulated cardiac fibroblasts. Circ Res. 69:116–122.

Chester AH, Taylor PM. 2007. Molecular and functional characteristics of heart-valve interstitial cells. Philos Trans R Soc Lond B Biol Sci. 362:1437–1443.

Choquet D, Felsenfeld DP, Sheetz MP. 1997. Extracellular matrix rigidity causes strengthening of integrin-cytoskeleton linkages. Cell. 88:39–48.

Cox MAJ, Kortsmit J, Driessen N, Bouten CVC, Baaijens FPT. 2010. Tissue-engineered heart valves develop native-like collagen fiber architecture. Tissue Eng Part A. 16:1527–1537.

Doehring TC, Kahelin M, Vesely I. 2005. Mesostructures of the aortic valve. J Heart Valve Dis. 14:679–686.

Durbin A, Nadir NA, Rosenthal A, Gotlieb AI. 2005. Nitric oxide promotes in vitro interstitial cell heart valve repair. Cardiovasc Pathol. 14:12–18.

Durbin AD, Gotlieb AI. 2002. Advances towards understanding heart valve response to injury. Cardiovasc Pathol. 11:69–77.

El Khoury G, Vanoverschelde JL, Glineur D, Pierard F, Verhelst RR, Rubay J, Funken JC, Watremez C, Astarci P, Lacroix V, et al., 2006. Repair of bicuspid aortic valves in patients with aortic regurgitation. Circulation. 114:I610–I616.

El Oakley R, Kleine P, Bach DS. 2008. Choice of prosthetic heart valve in today's practice. Circulation. 117:253–256.

Engelmayr GC, Jr, Hildebrand DK, Sutherland FW, Mayer JE, Jr, Sacks MS. 2003. A novel bioreactor for the dynamic flexural stimulation of tissue engineered heart valve biomaterials. Biomaterials. 24:2523–2532.

Engelmayr GC, Jr, Papworth GD, Watkins SC, Mayer JE, Jr, Sacks MS. 2006. Guidance of engineered tissue collagen orientation by large-scale scaffold microstructures. J Biomech. 39:1819–1831.

Engelmayr GC, Jr, Rabkin E, Sutherland FW, Schoen FJ, Mayer JE, Jr, Sacks MS. 2005. The independent role of cyclic flexure in the early in vitro development of an engineered heart valve tissue. Biomaterials. 26:175–187.

Fayet C, Bendeck MP, Gotlieb AI. 2007. Cardiac valve interstitial cells secrete fibronectin and form fibrillar adhesions in response to injury. Cardiovasc Pathol. 16:203–211.

Fung YC. 1993. Biomechanics: mechanical properties of living tissues. New York: Springer-Verlag.

Huang H-YS, Balhouse BN, Huang S. 2012. Application of simple biomechanical and biochemical tests to heart valve leaflets: implications for heart valve characterization and tissue engineering. Proc Inst Mech Eng Part H: J Eng Med. 226:868–876.

Huang H-YS, Liao J, Sacks MS. 2007. In-situ deformation of the aortic valve interstitial cell nucleus under diastolic loading. J Biomech Eng. 129:1–10.

Huang S, Huang H-YS. 2012. Virtual experiments of heart valve tissue. In: Mukkamala R, editor. IEEE Engineering in Medicine and Biology Society. San Diego (CA): IEEE. p. 6645–6648.

Huang S, Huang H-YS. 2013. Prediction of matrix-to-cell stress transfer in heart valve tissues. Med Eng Phys, under review.

Janmey PA, McCulloch CA. 2007. Cell mechanics: integrating cell responses to mechanical stimuli. Annu Rev of Biomed Eng. 9:1–34.

Joyce EM, Liao J, Schoen FJ, Mayer JE, Jr, Sacks MS. 2009. Functional collagen fiber architecture of the pulmonary heart valve cusp. Ann Thorac Surg. 87:1240–1249.

Koch TM, Reddy BD, Zilla P, Franz T. 2010. Aortic valve leaflet mechanical properties facilitate diastolic valve function. Comput Methods Biomech Biomed Eng. 13:225–234.

Langer SA, Fuller E, Carter WC. 2001. OOF: an image-based finite-element analysis of material microstructures. Comp Sci Eng. 3:15–23.

Langevin HM, Storch KN, Snapp RR, Bouffard NA, Badger GJ, Howe AK, Taatjes DJ. 2010. Tissue stretch induces nuclear remodeling in connective tissue fibroblasts. Histochem Cell Biol. 133:405–415.

Latif N, Sarathchandra P, Taylor PM, Antoniw J, Brand N, Yacoub MH. 2006. Characterization of molecules mediating cell–cell communication in human cardiac valve interstitial cells. Cell Biochem Biophys. 45:255–264.

Latif N, Sarathchandra P, Taylor PM, Antoniw J, Yacoub MH. 2005. Molecules mediating cell–ECM and cell–cell communication in human heart valves. Cell Biochem Biophys. 43:275–287.

Lewinsohn AD, Anssari-Benham A, Lee DA, Taylor PM, Chester AH, Yacoub MH, Screen HRC. 2011. Anisotropic strain transfer through the aortic valve and its relevance to the cellular mechanical environment. Proc Inst Mech Eng Part H: J Eng Med. 225:821–830.

Li J, Luo XY, Kuang ZB. 2001. A nonlinear anisotropic model for porcine aortic heart valves. J Biomech. 34:1279–1289.

Lim CT, Zhou EH, Quek ST. 2006. Mechanical models for living cells – a review. J Biomech. 39:195–216.

Liu AC, Joag VR, Gotlieb AI. 2007. The emerging role of valve interstitial cell phenotypes in regulating heart valve pathobiology. Am J Pathol. 171:1407–1418.

Luo XY, Li WG, Li J. 2003. Geometrical stress-reducing factors in the anisotropic porcine heart valves. J Biomech Eng. 125:735–744.

Mays PK, Bishop JE, Laurent GJ. 1988. Age-related changes in the proportion of type-I and type-III collagen. Mech Ageing Dev. 45:203–212.

Mendelson K, Schoen FJ. 2006. Heart valve tissue engineering: concepts, approaches, progress, and challenges. Ann Biomed Eng. 34:1799–1819.

Mohammadi H, Bahramian F, Wan W. 2009. Advanced modeling strategy for the analysis of heart valve leaflet tissue mechanics using high-order finite element method. Med Eng Phys. 31:1110–1117.

Mulholland DL, Gotlieb AI. 1996. Cell biology of valvular interstitial cells. Can J Cardiol. 12:231–236.

Mulholland DL, Gotlieb AI. 1997. Cardiac valve interstitial cells: regulator of valve structure and function. Cardiovasc Pathol. 6:167–174.

Nakagawa S, Pawelek P, Grinnell F. 1989. Extracellular-matrix organization modulates fibroblast growth and growth-factor responsiveness. Exp Cell Res. 182:572–582.

NIH. 2010. Heart and vascular diseases. Bethesda (MD): National Heart Lung and Blood Institute.

Nye JF. 1957. Physical properties of crystals, their representation by tensors and matrices. Oxford: Clarendon Press.

Park S, Koch D, Cardenas R, Kas J, Shih CK. 2005. Cell motility and local viscoelasticity of fibroblasts. Biophys J. 89:4330–4342.

Porter KE, Turner NA. 2009. Cardiac fibroblasts: at the heart of myocardial remodeling. Pharmacol Ther. 123:255–278.

Puklin-Faucher E, Sheetz MP. 2009. The mechanical integrin cycle. J Cell Sci. 122:179–186.

Reid ACE, Lua RC, Garcia RE, Coffman VR, Langer SA. 2009. Modelling microstructures with OOF2. Int J Mater Prod Technol. 35:361–373.

Roger VL, Go AS, Lloyd-Jones DM. 2012. Heart disease and stroke statistics – 2012 update – a report from the American Heart Association. Circulation. 125:E2–E220.

Sacks MS, Schoen FJ, Mayer JE, Jr. 2009. Bioengineering challenges for heart valve tissue engineering. Ann Rev Biomed Eng. 11:289–313.

Sacks MS, Smith DB, Hiester ED. 1998. The aortic valve microstructure: effects of transvalvular pressure. J Biomed Mater Res. 41:131–141.

Schwarzbauer JE. 1997. Cell migration: may the force be with you. Curr Biol. 7:R292–R294.

Sheetz MP, Felsenfeld DP, Galbraith CG. 1998. Cell migration: regulation of force on extracellular–matrix–integrin complexes. Trends Cell Biol. 8:51–54.

Slaughter WS. 2001. The linearized theory of elasticity. Boston (MA): Birkhauser.

Stella JA, Sacks MS. 2007. On the biaxial mechanical properties of the layers of the aortic valve leaflet. J Biomech Eng. 129:757–766.

Sun W, Sacks MS, Scott MJ. 2005. Effects of boundry conditions on the estimation of the planar biaxial mechanical properties of soft tissues. J Biomech Eng. 127:709–715.

Taylor PM, Allen SP, Dreger SA, Yacoub MH. 2002. Human cardiac valve interstitial cells in collagen sponge: a biological three-dimensional matrix for tissue engineering. J Heart Valve Dis. 11:298–307.

Taylor PM, Allen SP, Yacoub MH. 2000. Phenotypic and functional characterization of interstitial cells from human heart valves, pericardium and skin. J Heart Valve Dis. 9:150–158.

Taylor PM, Batten P, Brand NJ, Thomas PS, Yacoub MH. 2003. The cardiac valve interstitial cell. Int J Biochem Cell Biol. 35:113–118.

Yip CYY, Chen J-H, Zhao R, Simmons CA. 2009. Calcification by valve interstitial cells is regulated by the stiffness of the extracellular matrix. Arterioscler Thromb Vasc Biol. 29:936–942.